



## Article

# Physicochemical and Biological Evaluation of Chitosan-Coated Magnesium-Doped Hydroxyapatite Composite Layers Obtained by Vacuum Deposition

Daniela Predoi <sup>1,\*</sup>, Carmen Steluta Ciobanu <sup>1</sup> , Simona Liliana Iconaru <sup>1</sup> , Steinar Raaen <sup>2</sup> ,  
Monica Luminita Badea <sup>1,3</sup> and Krzysztof Rokosz <sup>4,\*</sup> 

<sup>1</sup> National Institute of Materials Physics, Atomistilor Street, No. 405A, P.O. Box MG 07, 077125 Magurele, Romania; ciobanucs@gmail.com (C.S.C.); simonaiconaru@gmail.com (S.L.I.); badea.artemisia@gmail.com (M.L.B.)

<sup>2</sup> Department of Physics, Norwegian University of Science and Technology (NTNU), Realfagbygget E3-124 Høgskoleringen 5, NO 7491 Trondheim, Norway; steinar.raaen@ntnu.no

<sup>3</sup> Faculty of Horticulture, University of Agronomic Sciences and Veterinary Medicine, 59 Marasti Blvd., 011464 Bucharest, Romania

<sup>4</sup> Division of Surface Electrochemistry & Technology, Faculty of Mechanical Engineering, Koszalin University of Technology, Raclawicka 15-17, PL 75-620 Koszalin, Poland

\* Correspondence: dpredoi@gmail.com (D.P.); krzysztof.rokosz@wp.pl (K.R.)

**Abstract:** In the present work, the effectiveness of vacuum deposition technique for obtaining composite thin films based on chitosan-coated magnesium-doped hydroxyapatite  $\text{Ca}_{10-x}\text{Mg}_x(\text{PO}_4)_6(\text{OH})_2$  with  $x_{\text{Mg}} = 0.025$  (MgHApCh) was proved for the first time. The prepared samples were exposed to three doses (0, 3, and 6 Gy) of gamma irradiation. The MgHApCh composite thin films nonirradiated and irradiated were evaluated by scanning electron microscopy (SEM), atomic force microscopy (AFM), and X-ray photoelectron spectroscopy (XPS) studies. The biological evaluation of the samples was also presented. All the results obtained from this study showed that the vacuum deposition method allowed for obtaining uniform and homogeneous layers. Fine cracks were observed on the MgHApCh composite thin films' surface after exposure to a 6 Gy irradiation dose. Additionally, after gamma irradiation, a decrease in Ca, P, and Mg content was noticed. The MgHApCh composite thin films with doses of 0 and 3 Gy of gamma irradiation showed a cellular viability similar to that of the control. Samples with 6 Gy doses of gamma irradiation did not cause significantly higher fibroblast cell death than the control ( $p > 0.05$ ). On the other hand, the homogeneous distribution of pores that appeared on the surface of coatings after 6 Gy doses of gamma irradiation did not prevent the adhesion of fibroblast cells and their spread on the coatings. In conclusion, we could say that the thin films could be suitable both for use in bone implants and for other orthopedic and dentistry applications.

**Keywords:** vacuum deposition; chitosan-coated magnesium-doped hydroxyapatite; gamma irradiation; surface morphology; chemical composition; biocompatibility



**Citation:** Predoi, D.; Ciobanu, C.S.; Iconaru, S.L.; Raaen, S.; Badea, M.L.; Rokosz, K. Physicochemical and Biological Evaluation of Chitosan-Coated Magnesium-Doped Hydroxyapatite Composite Layers Obtained by Vacuum Deposition. *Coatings* **2022**, *12*, 702. <https://doi.org/10.3390/coatings12050702>

Academic Editor: Devis Bellucci

Received: 14 April 2022

Accepted: 18 May 2022

Published: 20 May 2022

**Publisher's Note:** MDPI stays neutral with regard to jurisdictional claims in published maps and institutional affiliations.



**Copyright:** © 2022 by the authors. Licensee MDPI, Basel, Switzerland. This article is an open access article distributed under the terms and conditions of the Creative Commons Attribution (CC BY) license (<https://creativecommons.org/licenses/by/4.0/>).

## 1. Introduction

Nowadays, the interest of the scientific community to develop new nanocomposite materials with potential applications in the biomedical field is increasing due to the unique properties of these compounds [1–8]. Recent studies conducted by Mousavi and collaborators [1–15] propose various types of nanocomposite materials for uses in domains such as anticancer and antibacterial applications, tissue engineering, gene therapy and drug delivery, and bioimaging. In the last decade, hydroxyapatite (HAp) has been one of the most studied biomaterials by researchers worldwide. The chemical formula of HAp is  $\text{Ca}_{10}(\text{PO}_4)_6(\text{OH})_2$ , and the molar ratio Ca/P is equal to 1.67. Moreover, hydroxyapatite is the main inorganic part that is found in bone and teeth tissues of humans and animals [16].

Previous studies reported interesting results regarding HAp's biological properties, such as biocompatibility, bioactivity, nontoxicity, and osteoconductivity [17,18]. Due to these good biological properties, HAp has been used in many applications from the biomedical domain, as well as other domains. On the other hand, one of the most studied natural polymers (polysaccharide) is represented by chitosan and its derivatives. The areas of application of chitosan include domains of interest for researchers around the world, such as pharmaceutical and biomedical domains [19,20]. The use of chitosan in these domains is mainly due to its good biological activity (e.g., biocompatibility, biodegradability, antimicrobial activity) [21]. Due to its weak mechanical strength and solubility, the applicability of HAp is limited. A solution to overcome this weakness is represented by the doping of hydroxyapatite with various ions, such as silver, magnesium, zinc, strontium, europium, and cerium [22–26]. Magnesium ( $Mg^{2+}$ ) is one of the most abundant chemical elements that can be found in mammals and has the ability to easily substitute calcium from the HAp structure due to its high affinity [27]. Furthermore, it has been highlighted that magnesium ions can play an important role in various bone processes, such as crystallization, formation, and metabolism [28]. Suboptimal levels of magnesium in the human body could lead to decreased bone density [22]. Moreover, previous studies have shown that by doping hydroxyapatite with magnesium ions (MgHAp), biomaterials with a positive impact on bone mineralization [29] could be obtained. An important role in the biological and antimicrobial activity of magnesium-doped hydroxyapatite compounds is played by the concentration of magnesium in the samples. Thus, it is extremely important to find the optimal concentration of magnesium that will produce maximum positive biological effects [29,30]. Given these unique properties of magnesium ions, we chose to dope hydroxyapatite with a low concentration of  $Mg^{2+}$ . More than that, it has been proved that high amounts of magnesium can cause unwanted biological effects [29]. The use of chitosan as a matrix for doped hydroxyapatite may represent a valuable solution in order to obtain new biomaterials with improved biological activity and solubility [31]. Therefore, the new compounds obtained by the development of MgHAp in a chitosan matrix could own enhanced biological and antimicrobial properties [30]. For the deposition of hydroxyapatite composite thin films, various techniques, such as spin coating [32,33], vacuum deposition [34], PLD (pulsed laser deposition) [35], and RF magnetron sputtering [36], are currently available. Among these techniques, vacuum deposition spin coating produces uniform thin films [37]. In a study conducted by Teng and collaborators [38], it was highlighted that the presence of chitosan, in a three-layered membrane based on collagen/HAp/chitosan, has a major contribution to the improvement of the physicochemical properties of the studied materials. The biological activity of hydroxyapatite/chitosan composite biomaterials was evaluated by *in vitro* assays using various cell lines. For example, chitosan/hydroxyapatite/magnetite composite showed an enhanced bioactivity by supporting osteoblast cell adhesion and proliferation [39]. Furthermore, cytotoxicity studies conducted by Sutha et al. [33] on a fibroblast cell line showed that magnesium-doped hydroxyapatite/chitosan composite exhibited less toxicity compared with hydroxyapatite/chitosan composite. In previous studies, it has been proved that the doping ions and the chitosan matrix's stiffness and roughness influence the proliferative capacity of ME3T3-E1 cells [22]. Additionally, an enhanced biocompatibility of chitosan coatings was noticed in the case of human lung fibroblast cells [40]. Before being used in various applications, biomaterials require sterilization, and a common method is to use ionizing radiation. Exposure to  $\gamma$ -irradiation of an inorganic/organic mixture may lead to some effects that need to be carefully studied (such as improved crystallization, surface modification) [41]. Thus, it is highlighted that the adhesions and proliferation rate of osteoblast cell were highly improved by exposure to  $\gamma$ -irradiation of carbon-dot-decorated polyethylene-gold@hydroxyapatite biocomposite on titanium [42]. In our previous papers, we presented results obtained on hydroxyapatite-polydimethylsiloxane layers exposed at 2 Gy (X-ray radiation dose) [43]. Our previous results highlight both compositional and morphological changes in the analyzed samples [30,43]. Furthermore, similar effects were noticed after exposure to UV radiation of silver-doped hydroxyapatite thin films [34].

In this paper, we report for the first time the development of chitosan-coated magnesium-doped hydroxyapatite thin films (MgHApCh) by vacuum deposition method. The obtained samples were  $\gamma$ -irradiated, and we studied the physicochemical and biological properties before and after  $\gamma$ -irradiation. The structure of MgHApCh thin films was studied by X-ray diffraction (XRD). Furthermore, the vibrational bands presented in MgHApCh composite thin films were analyzed using Fourier-transform infrared spectroscopy (FTIR). The surface morphology of MgHApCh thin films was studied by scanning electron microscopy (SEM), atomic force microscopy (AFM), and X-ray photoelectron spectroscopy (XPS). Additionally, the biocompatibility of the unirradiated and irradiated composite thin films was achieved using fibroblast cells. Based on our results, we could say that the thin films could be suitable both for use in bone implants and for other orthopedic and dentistry applications.

## 2. Materials and Methods

### 2.1. Materials

The powders of chitosan-coated magnesium-doped hydroxyapatite  $\text{Ca}_{10-x}\text{Mg}_x(\text{PO}_4)_6(\text{OH})_2$  with  $x_{\text{Mg}} = 0.025$  (MgHApCh) were obtained using calcium nitrate tetrahydrate ( $\text{Ca}(\text{NO}_3)_2 \cdot 4\text{H}_2\text{O}$ ; Sigma-Aldrich, St. Louis, MO, USA,  $\geq 99.0\%$ ), magnesium nitrate hexahydrate ( $\text{Mg}(\text{NO}_3)_2 \cdot 6\text{H}_2\text{O}$ ; Alfa Aesar, Germany, 99.97% purity),  $(\text{NH}_4)_2\text{HPO}_4$  (Sigma-Aldrich, St. Louis, MO, USA,  $\geq 99.0\%$ ); ammonium hydroxide ( $\text{NH}_4\text{OH}$ ; Sigma-Aldrich, St. Louis, MO, USA, 25%  $\text{NH}_3$  in  $\text{H}_2\text{O}$  (T)), chitosan ( $\text{C}_6\text{H}_{11}\text{NO}_4$ ), ethanol absolute ( $\text{C}_2\text{H}_5\text{OH}$ ), and double-distilled water.

### 2.2. Chitosan-Coated Magnesium-Doped Hydroxyapatite (MgHApCh)

The powders of chitosan-coated magnesium-doped hydroxyapatite  $\text{Ca}_{10-x}\text{Mg}_x(\text{PO}_4)_6(\text{OH})_2$  with  $x_{\text{Mg}} = 0.025$  (MgHApCh) were achieved in accord with precedent studies [44–46]. The molar ratio for this experiment was 1.67. The pH was kept at 11 during the synthesis. The coprecipitation of  $\text{Ca}(\text{NO}_3)_2 \cdot 4\text{H}_2\text{O}$  and  $\text{Mg}(\text{NO}_3)_2 \cdot 6\text{H}_2\text{O}$  solution in  $(\text{NH}_4)_2\text{HPO}_4$  and  $\text{C}_6\text{H}_{11}\text{NO}_4$  was performed under continuous stirring at  $100^\circ\text{C}$ . The final suspensions obtained after 4 h were centrifuged and redispersed in deionized water under continuous stirring at  $100^\circ\text{C}$ . The final precipitate obtained was dried in an oven at  $100^\circ\text{C}$  in the air. The MgHApCh powder was used in order to obtain the MgHApCh composite coatings.

### 2.3. Preparation of Chitosan-Coated Magnesium-Doped Hydroxyapatite Layers

The MgHApCh composite thin films were deposited on silicon substrates. Before the deposition process, the silicon substrates were cleaned by rinsing with acetone several times. The silicon substrates were dried at  $40^\circ\text{C}$ . The MgHApCh nanopowder was used to achieve the MgHApCh thin films by vacuum deposition. The conditions for obtaining the coatings were a medium pressure of  $p \sim 6.5 \times 10^{-5}$  torr, a maximum current intensity of  $I = 150$  A, and an evaporation time of around 150 s. The MgHApCh composite thin films were exposed to doses of 0 (MgHApCh-0), 3 Gy (MgHApCh-3), and 6 Gy (MgHApCh-6) of gamma irradiation.

### 2.4. Physicochemical Characterizations

The MgHApCh composite thin films (before and after exposure to gamma irradiation) were examined by X-ray diffraction (XRD) using a Bruker D8 Advance diffractometer (Billerica, MA, USA) equipped with nickel-filtered  $\text{Cu K}\alpha$  ( $\lambda = 1.5418 \text{ \AA}$ ) radiation.

Scanning electron microscopy (SEM) investigations of MgHApCh composite thin films nonirradiated and irradiated were performed using a Hitachi S4500 scanning electron microscope (Hitachi, Tokyo, Japan). The elemental composition of the films by energy dispersive X-ray spectroscopy (EDX) was effectuated using an energy dispersive X-ray (EDX) detection system attached to the microscope. The surfaces of MgHApCh composite thin films were analyzed without spraying them with vacuum silver or gold. Moreover, with the aid of ImageJ software [47], the 3D representation of the SEM images was achieved.

Additional information concerning the morphology and roughness of MgHApCh composite thin films was achieved using an NT-MDT Ntegra Probe Nano Laboratory instrument (NT-MDT, Moscow, Russia) atomic force microscope. The atomic force microscope that was used operated in semicontact mode (using a silicon NT-MDT NSG01 cantilever (NT-MDT, Moscow, Russia) coated with a 35 nm gold layer). The atomic force microscopy (AFM) images of MgHApCh composite thin films were acquired for a surface area of  $2.5 \times 2.5 \mu\text{m}^2$ . The acquired data were processed with Gwyddion 2.59 software (Department of Nanometrology, Czech Metrology Institute, Brno, Czech Republic) [48].

The X-ray photoelectron spectroscopy (XPS) investigation was realized with a SES 2002 instrument (Scienta Omicron) using a monochromatic Al K(alpha) ( $h\nu = 1486.6 \text{ eV}$ ) X-ray source (Scienta Omicron, 18.7 mA, 13.02 kV). Scan analyses were carried out in agreement with previous studies [49,50]. The experiments were performed in accordance with the last studies [49,50]. The CasaXPS 2.3.14 software (Shirley background type) [51] was used in order to analyze the XPS data. The XPS tables [52,53] were used too. All the binding energy (BE) values presented in this study were charge-corrected to C 1s at 284.8 eV.

Fourier-transform infrared (FTIR) spectroscopy was used in order to investigate functional groups present in the MgHApCh composite thin films. The FTIR studies were conducted with a PerkinElmer Spectrum BX II spectrometer equipped with a Pike MIRacle ATR (attenuated total reflectance) head. The FTIR spectra were recorded in the spectral domain  $450\text{--}1800 \text{ cm}^{-1}$  with a resolution of  $4 \text{ cm}^{-1}$ .

The adhesion of the studied samples (unirradiated and irradiated) to the silicon substrate was studied using tape-pull test with the aid of a 3M Performance Flatback Tape 2525 tape. The peel adhesion was 7.5 N/cm.

### 2.5. Biological Evaluation

The biological activity of the unirradiated and irradiated MgHApCh composite thin films (with 3 and 6 Gy irradiation doses) was assessed using a human fibroblast cell line. For this purpose, the MgHApCh composite thin films were incubated for a period of 24 h with a human fibroblast cell line. The fibroblast cells having a density of  $5 \times 10^4$  cells per well were seeded in an atmosphere containing 5%  $\text{CO}_2$  at  $37 \text{ }^\circ\text{C}$ . The procedure is described in details in our previous work [54]. The human fibroblast cell viability after being incubated for 24 h with the MgHApCh composite thin films was evaluated using 3-(4,5-dimethylthiazol-2-yl)-2,5-diphenyltetrazolium bromide (MTT) assay. After 24 h of incubation with the MgHApCh composite thin films, the environment was removed by aspiration, and afterwards, the cultured human fibroblasts were incubated for 2 h with 1 mg/mL MTT solution. A solution containing 2-propanol was used in order to dissolve the purple formazan crystals. The absorbance at 595 nm was obtained with the aid of a GENiosTecan microplate reader (GENiosTecan, Salzburg, Austria) [54]. Furthermore, the fibroblast cell morphology and their adherence and proliferation on the surface of MgHApCh composite thin films were studied using AFM. For this purpose, the cells were fixed with 4% paraformaldehyde for 20 min and permeabilized with 0.1% Triton X-100—2% bovine serum albumin for 1 h. The experiments were performed in triplicate, and all the results were expressed as mean value  $\pm$  SD. Statistical analysis was performed using the standard *t*-test. Values of  $p < 0.05$  were considered statistically significant.

## 3. Results

In Figure 1 are presented the standard card of the HAp (ICDD-PDF #9-0432) and XRD patterns of the unirradiated (Figure 1b) and 6 Gy irradiated (Figure 1c) MgHApCh composite layers. The peaks identified from XRD patterns of the unirradiated (Figure 1b) and 6 Gy irradiated (Figure 1c) MgHApCh composite layers were in good agreement with the standard card of HAp (Figure 1a). The peak broadening of the MgHApCh-6 layers increased compared with the unirradiated sample (Figure 1b). The XRD analysis revealed that the crystallinity of the irradiated samples decreased. The XRD results were in agreement with the SEM and FTIR studies.

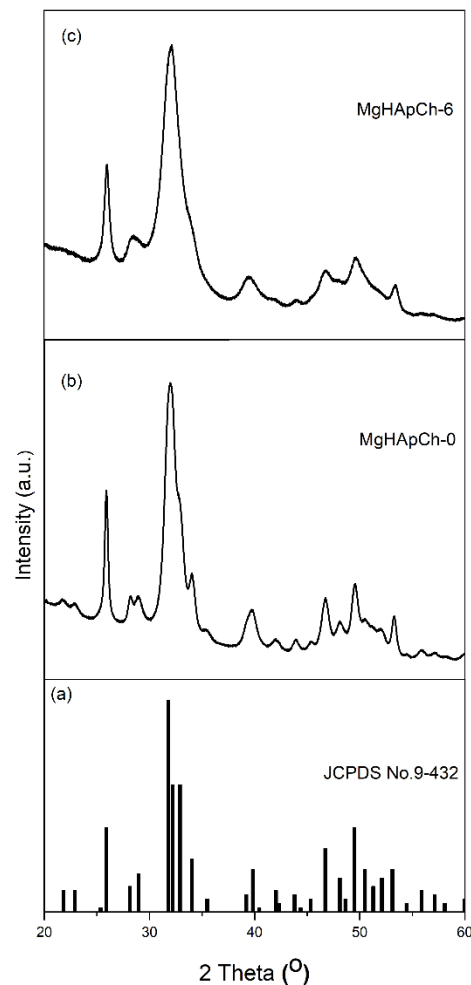


**Figure 1.** XRD patterns of MgHApCh-0 (b) and MgHApCh-6 (c) composite coatings along with the standard card of the HAp (ICDD-PDF #9-0432) (a).

The surface morphology of the MgHApCh composite coatings, namely, MgHApCh-0, MgHApCh-3, and MgHApCh-6, was studied by scanning electron microscopy technique. The 2D and 3D representations of the obtained SEM micrographs are presented in Figure 2.

In Figure 2, it can be observed that the surface morphology of the studied sample is slightly influenced after the irradiation with higher doses (6 Gy). More than that, the sample roughness increases with the increase in radiation dose to which the coatings were exposed. The surface of the composite thin films obtained by vacuum deposition method seems to be nanostructured (Figure 2a). The exposure of MgHApCh composite coatings at various irradiation doses (as can be seen in Figure 2c,e) induces an increase in surface nanostructuration. The presence of fine cracks could be observed in the case of the MgHApCh-6 sample.

Moreover, the surface uniformity and homogeneity seem to be preserved for all the samples. Using the ImageJ software (ImageJ 1.51j8, National Institutes of Health, Bethesda, MD, USA), the 3D representation of 2D SEM micrographs (Figure 2b,d,f) was obtained for a better observation of the surface characteristics. Our results are in good agreement with the ones reported in a study conducted by Bitá and collaborators [30].

The quantitative and qualitative chemical compositions along with the elemental distribution of the constituent elements in the MgHApCh-0 composite coatings were studied with the aid of energy dispersive X-ray spectroscopy (EDX). The results of the EDX studies are also shown in Figure 3.

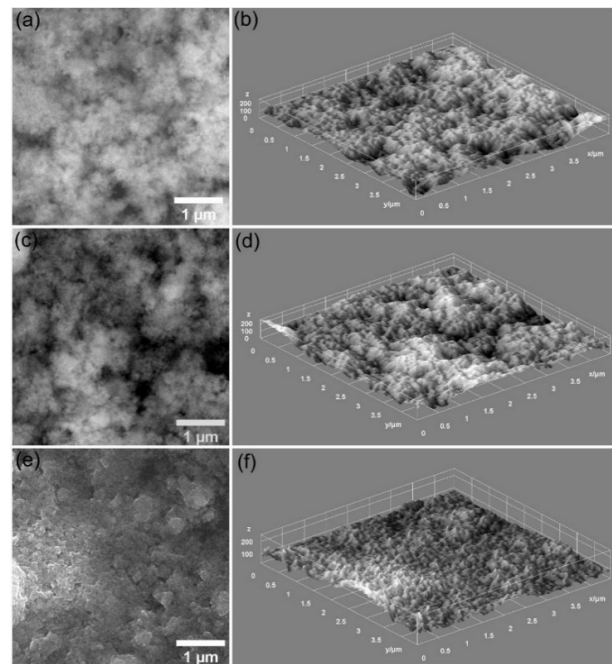


**Figure 2.** SEM characteristic micrographs of MgHApCh-0 (a), MgHApCh-3 (c), and MgHApCh-6 (e) composite coatings. The 3D representation of SEM micrographs obtained for MgHApCh-0 (b), MgHApCh-3 (d), and MgHApCh-6 (f) composite coatings.

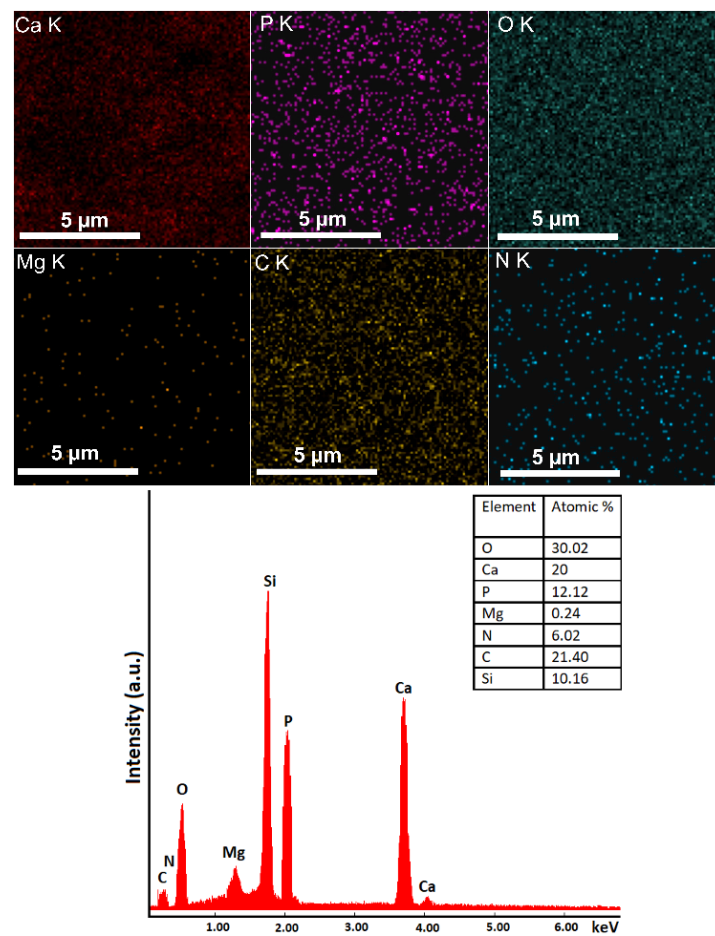


**Figure 3.** Elemental mapping of constituent elements and EDX spectra of MgHApCh-0 composite coatings.

The results of EDX studies reveal the presence of the main constituent elements (calcium, phosphorus, oxygen, magnesium, carbon, and nitrogen) in the investigated coatings. The presence of carbon and nitrogen lines in the EDX spectra is specific to chitosan. Additionally, the line of silicon from the EDX spectra arises from the substrate on which the composite layers were deposited by vacuum deposition technique. Elemental mapping revealed the homogenous and uniform distribution of calcium, phosphorus, oxygen, magnesium, carbon, and nitrogen in the MgHApCh-0 composite thin films.

The SEM micrographs of the transversal cross section of MgHApCh layers, presented in Figure 4, indicated the layer thickness. It could be noticed that the thickness of MgHApCh-0 layers was around 105 nm, and in the case of the MgHApCh-3 sample, a layer thickness of around 104 nm was obtained. Meanwhile, the thickness of MgHApCh-6 coatings was around 103 nm.

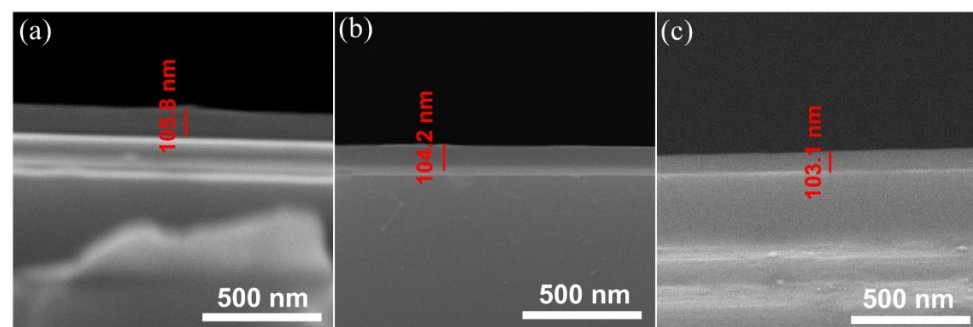


**Figure 4.** SEM micrographs of the transversal cross section of MgHApCh-0 (a), MgHApCh-3 (b), and MgHApCh-6 (c) composite coatings.

The adherence strength of the unirradiated and irradiated MgHApCh thin films to the Si substrate was studied with the aid of a common tape-pull test. Therefore, for all the studied samples, the Scotch tape came off relatively clean. Moreover, the substrate surface analysis indicated that MgHApCh thin films were unbroken. Our results highlight that MgHApCh thin films (unirradiated and irradiated) have a good adherence to the Si substrate.

Supplementary information about the surface topography of the MgHApCh-0, MgHApCh-3, and MgHApCh-6 composite thin films was obtained by conducting atomic force microscopy (AFM) studies. The results of AFM studies are reported in Figure 5a,c,e (2D AFM images). Additionally, the 3D representation of the 2D AFM images is presented in Figure 5b,d,f.

The AFM studies revealed similar surface topographies as those obtained from SEM studies. Thus, the presence of a continuous, homogenous, and structured surface was noticed. An increase in surface porosity was pointed out after exposure at higher irradiation doses (6 Gy) of MgHApCh. Moreover, in the case of MgHApCh-0 and MgHApCh-3, samples highlighted the absence of fissures and cracks on the coating surfaces. Meanwhile, after an irradiation with 6 Gy of MgHApCh coatings, the appearance of fine cracks could be distinguished. No other surface defects were noticed on the studied coating surface.

The modification of surface roughness with the increase in  $\gamma$ -irradiation doses was highlighted also by the root mean square ( $R_{RMS}$ ) parameter values determined for the studied samples. Therefore, for the unirradiated sample MgHApCh-0, the value of the  $R_{RMS}$  parameter was equal to 38.86 nm. For the MgHApCh-3 composite coatings was obtained a  $R_{RMS}$  value equal to 42.37 nm, while for the MgHApCh-6 sample, an  $R_{RMS}$  value equal to 49.31 nm was obtained. Thus, it was observed that with the increase of irradiation dose, the surface roughness also increases. Thus, it could be observed that the results regarding the surface topography/morphology obtained by AFM studies are in good agreement with the one obtained by SEM studies.

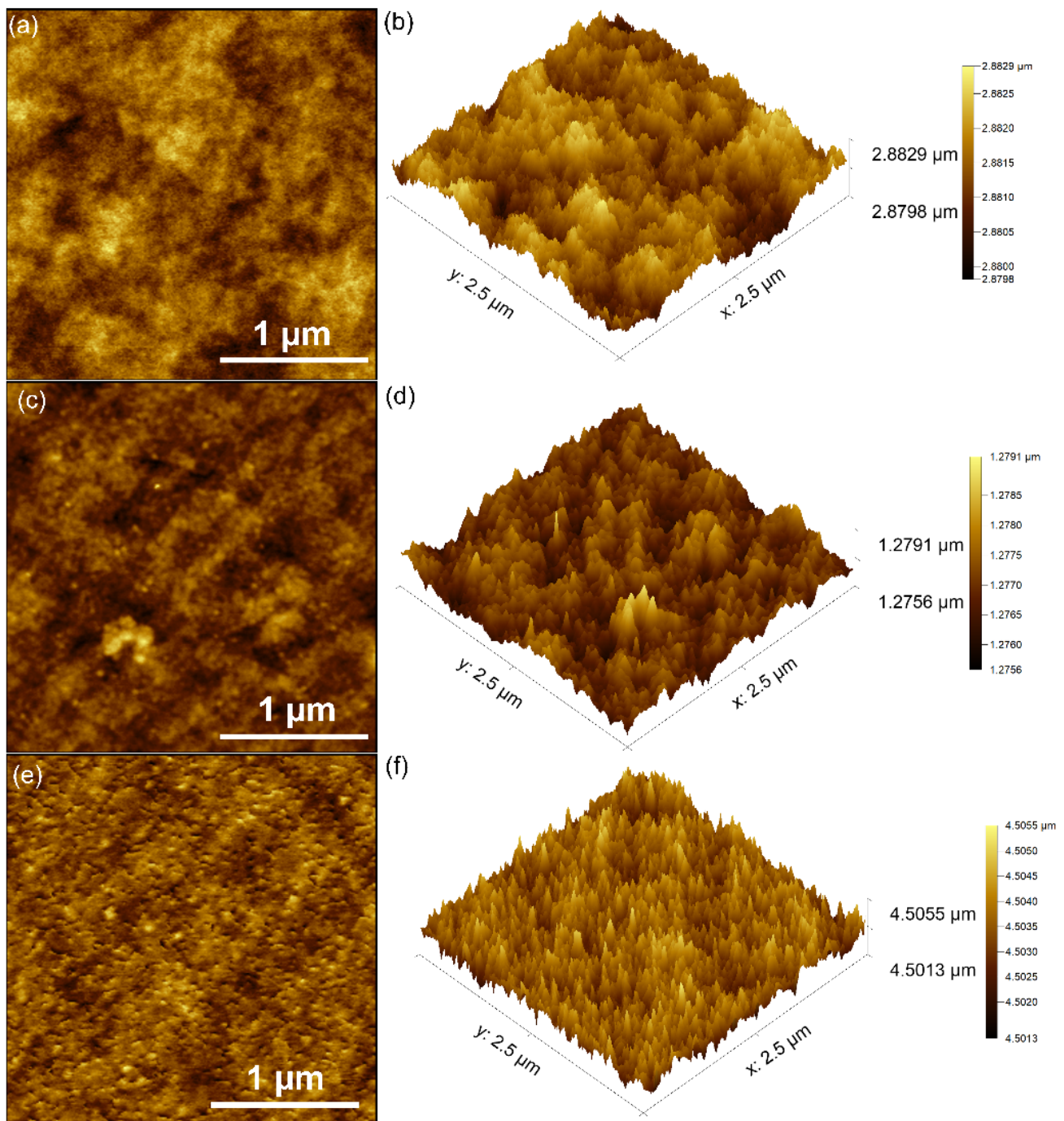


**Figure 5.** Two-dimensional AFM images of MgHApCh-0 (a), MgHApCh-3 (c), and MgHApCh-6 (e) composite coatings. Three-dimensional AFM images obtained for MgHApCh-0 (b), MgHApCh-3 (d), and MgHApCh-6 (f) composite coatings.

The XPS investigations of MgHApCh composite thin film nonirradiated and irradiated with irradiation doses of 0, 3, and 6 Gy of gamma irradiation were effectuated in order to evaluate the doping of hydroxyapatite with magnesium ions and the effect of the irradiation process. As a result of these studies, the presence of the magnesium ions in the surface was highlighted in all the analyzed samples. The survey results before and after argon etching for examined samples are presented in Figures 6 and 7. In the general XPS spectrum of the MgHApCh composite thin film nonirradiated and irradiated recorded before etching (Figure 6), the constituent elements of the analyzed sample (Ca, P, O, Mg (1s), and Mg



(KLL)) were identified. The signal registered for C1s was due to the reference carbon at a binding energy (BE) of 289.5 eV before etching. The XPS results for Ca 2p, P2p, O 1s, Mg 1s, and Mg KLL spectra before argon etching for MgHApCh-0, MgHApCh-3, and MgHApCh-6 composite thin films are presented in Figures 8 and 9.

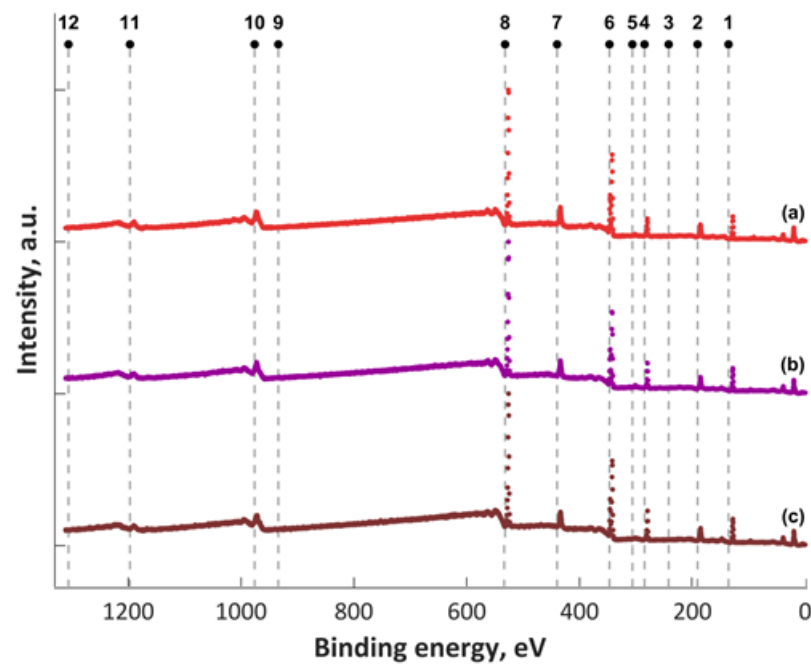


Figure 6. XPS survey results before argon etching for MgHApCh-0 (a), MgHApCh-3 (b), and MgHApCh-6 (c).

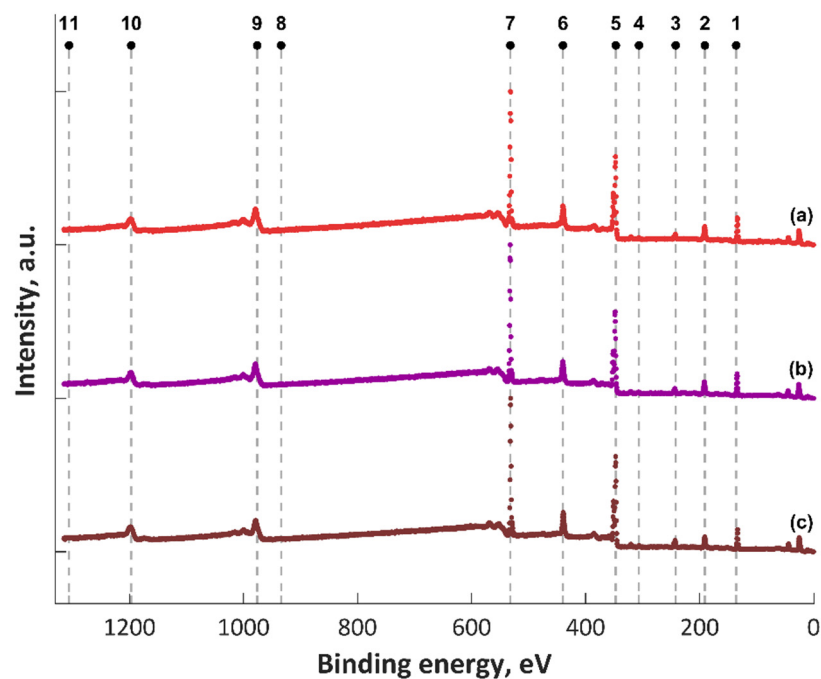
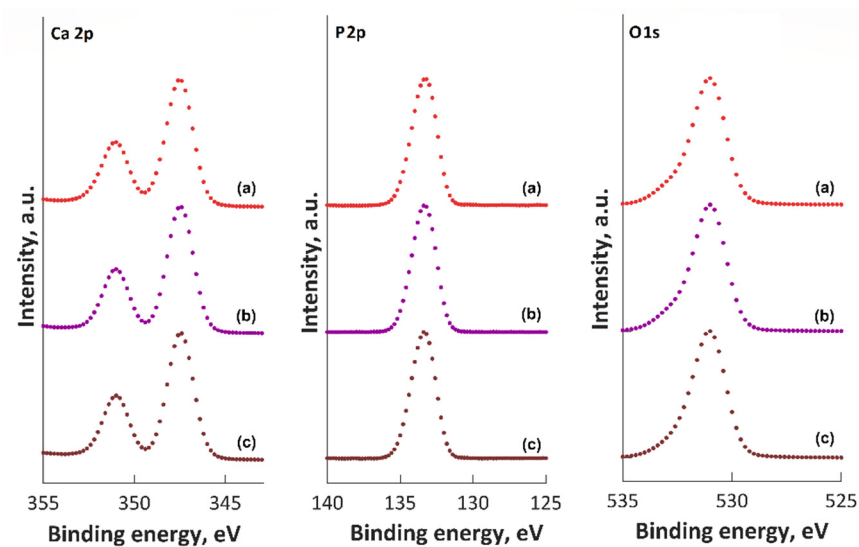
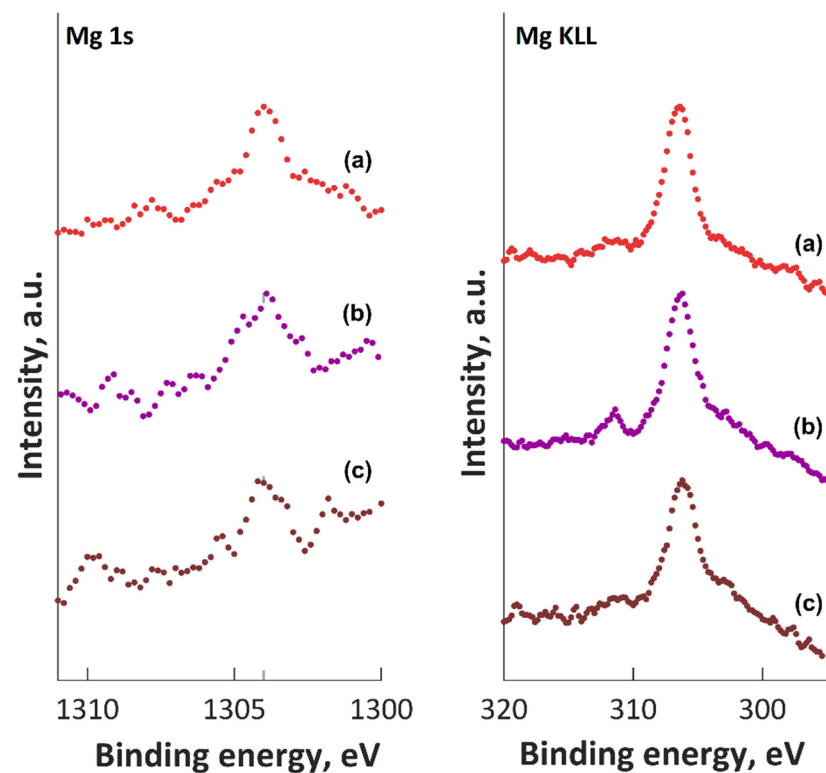


Figure 7. XPS survey results after argon etching for MgHApCh-0 (a), MgHApCh-3 (b), and MgHApCh-6 (c) composite thin films.



**Figure 8.** XPS results for Ca 2p, P 2p, and O 1s spectra before argon etching for MgHApCh-0 (a), MgHApCh-3 (b), and MgHApCh-6 (c) composite thin films.



**Figure 9.** XPS results for Mg 1s and Mg KLL spectra before argon etching for MgHApCh-0 (a), MgHApCh-3 (b), and MgHApCh-6 (c) composite thin films.

The XPS results suggest that the top layer of the MgHApCh composite thin film nonirradiated (MgHApCh-0) contains magnesium ( $Mg^{2+}$ ) and calcium ( $Ca^{2+}$ ) from hydroxyapatite. For the MgHApCh-0 composite thin film, the BE of Ca 2p, P 2p, and O 1s signal is in good accord with the value presented for hydroxyapatite (HAp) in previously reported studies [55–57]. The main peak of the O 1s XPS spectra before argon etching was located at 531.2 eV and is assigned to HAp [55–57]. On the other hand, the BE of P 2p signal (133.2 eV) and the peak located at BE at about 347.3 eV that was assigned to Ca 2p are in good accordance with the value previously reported for HAp [55–57]. The Mg 1s and Mg KLL peak positions for the MgHApCh-0 sample were located at BEs of 1302 and 304.3 eV.

The XPS results for Ca 2p, P2p, O 1s spectra before argon etching for MgHApCh-3 and MgHApCh-6 composite thin films presented in Figure 8 show a slight peak shift with the increase in irradiation dose. The XPS results for MgHApCh composite thin film irradiated with irradiation doses of 3 and 6 Gy suggest that the top layer contains magnesium ( $Mg^{2+}$ ) and calcium ( $Ca^{2+}$ ) from hydroxyapatite and tricalcium phosphate (TCP;  $Ca_3(PO_4)_2$ ). The peak position of Ca 2p was at around 347.50 eV for MgHApCh-3 composite thin films, while the BE of Ca 2p for MgHApCh-6 composite thin films was located at 347.71 eV. The binding energies for P2p for MgHApCh-3 and MgHApCh-6 composite thin films were located at around 133.4 and 133.64 eV, respectively. The peak positions of O 1s for MgHApCh-3 and MgHApCh-6 composite thin films were 531.28 and 531.34 eV. The Mg 1s and Mg KLL peak positions for the MgHApCh-3 sample were observed at about 1302.93 and 305.1 eV. For MgHApCh-6, the Mg 1s and Mg KLL peak positions were located at BEs of 1304 and 306 eV. The XPS results for MgHApCh-6 composite thin film suggested an increase in the amount of TCP in the top layer. The tendency of the binding energies' changes is in good agreement with the irradiation process of the coating, suggesting an increase in the amount of TCP in the upper layer of the MgHApCh-3 and MgHApCh-6 samples [58–60].

The results of the ATR–FTIR studies conducted on unirradiated and irradiated MgHApCh coatings are shown in Figure 10.

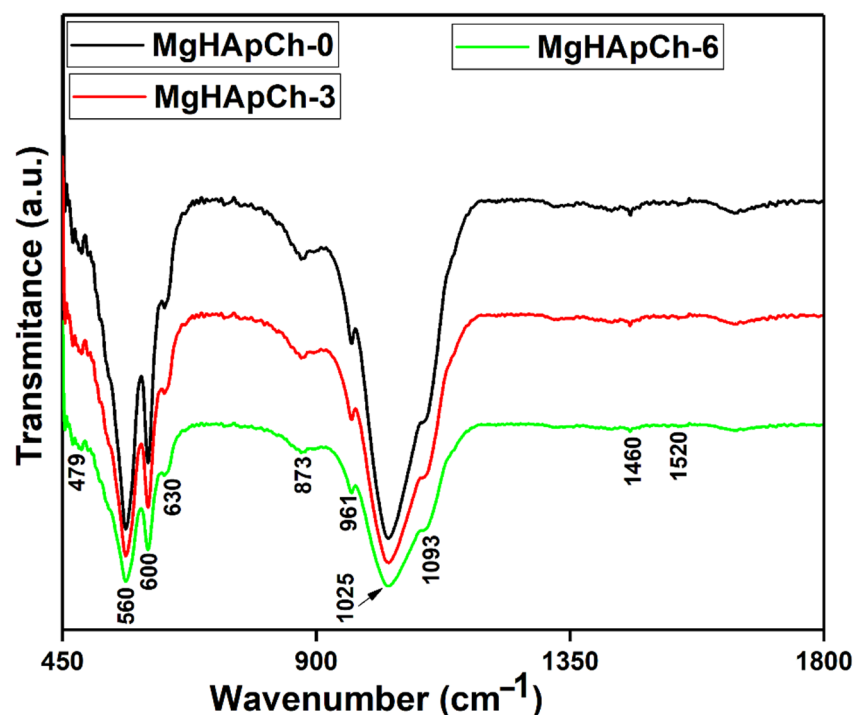
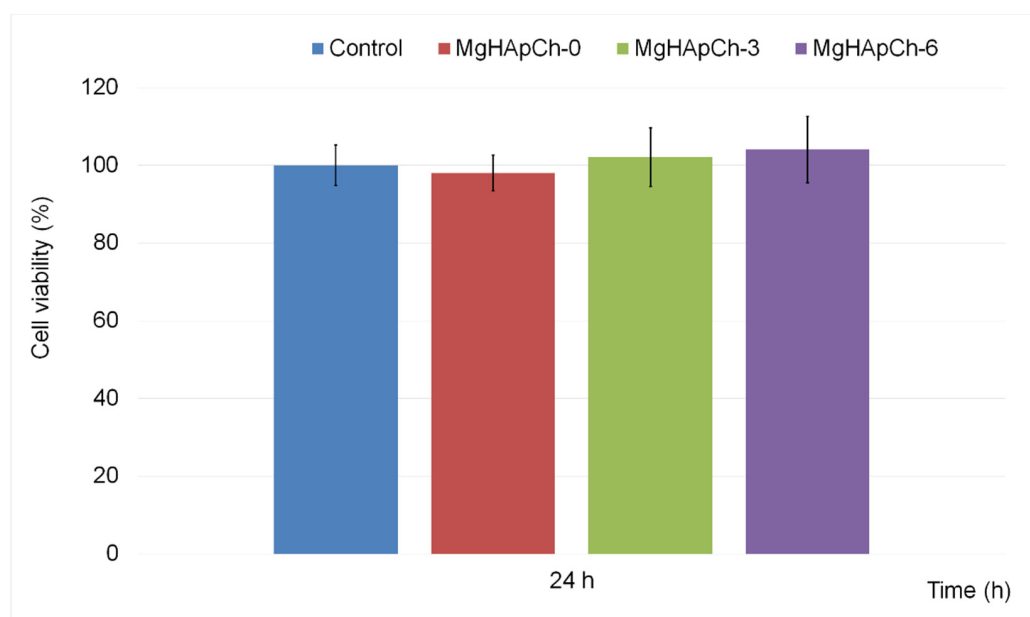


Figure 10. ATR–FTIR spectra of MgHApCh-0, MgHApCh-3, and MgHApCh-6 composite thin films.

Therefore, in the FTIR spectra could be noticed the presence of vibrational bands characteristic P–O vibration in phosphate groups and C–H/C–O vibration in the chitosan structure. The main vibration bands associated with phosphate groups due to symmetric stretching ( $\nu_1$ ) are at around 940–980  $cm^{-1}$  [61]. The bands associated with the triple-degenerate asymmetric stretching of P–O vibration in phosphate groups ( $\nu_3$ ) are between 1000 and 1100  $cm^{-1}$  [61]. The maxima that belong to double-degenerate bending ( $\nu_2$ ) are between 400 and 500  $cm^{-1}$ , and those of triple-degenerate ( $\nu_4$ ) of P–O vibration in phosphate groups could be found in the 550–600  $cm^{-1}$  spectral domain [61]. The vibrational bands that are found in the 1300–1800  $cm^{-1}$  spectral domain are mainly attributed to N–H, C–H, C–O, and C=O vibration in chitosan structure [34]. Moreover, the FTIR results suggest that with the increase in radiation dose from 3 to 6 Gy, the maxima are slightly displaced and become more broadened.

The biological properties of the MgHApCh composite thin films (MgHApCh-0, MgHApCh-3, MgHApCh-6) were investigated through *in vitro* studies with the aid of a human fibroblast cell line. The *in vitro* assays were performed in triplicate, and the cell viability of the fibroblast cells incubated with the MgHApCh composite thin films was assessed after 24 h of incubation. The results of the MTT tests are depicted in Figure 11. A human fibroblast cell culture was grown without being incubated with MgHApCh composite thin films and used as control. The MTT assay results emphasized that MgHApCh composite thin films exhibited good biocompatibility compared with the control cell culture after a period of 24 h of incubation. Moreover, the results of the MTT assay highlighted that after 24 h of incubation, the fibroblast cell viability was above 98% and had an increasing tendency correlated with the gamma irradiation dose, reaching a viability of approximately  $102 \pm 7.56\%$  for the sample irradiated with a dose of 3 Gy and  $104 \pm 8.58\%$  for the sample irradiated with a dose of 6 Gy. The results of the *in vitro* cell viability assay depicted that all the tested MgHApCh composite thin films exhibited good viability against human fibroblast cells after a period of 24 h of incubation. Moreover, the data also suggested that the irradiation dose prior applied to the composite thin films had a positive influence on the fibroblast cell viability. Considering these results, we can conclude that the MgHApCh composite thin films exhibited good biocompatibility and could further be considered for the development of biomedical devices.



**Figure 11.** Cell viability of human fibroblast cells after 24 h of incubation with MgHApCh composite thin films. Results are presented as mean  $\pm$  standard deviation (SD) and quantified in relation to control (100%, untreated cells).

Supplementary information regarding the adherence, proliferation, and biocompatibility of human fibroblast cells on the surface of MgHApCh composite thin films after 24 h of incubation was obtained using AFM technique. The AFM topographies were recorded on MgHApCh composite thin films' surface of  $40 \times 40 \mu\text{m}^2$  at room temperature in normal atmospheric conditions. The AFM topographies of the fibroblast cells adhered to the surfaces of MgHApCh composite thin films unirradiated and irradiated after 24 h of incubation are presented in Figure 12a–f. The 2D topographies of the fibroblast cells adhered to the surface of unirradiated MgHApCh composite thin films after 24 h of incubation and their 3D representation are depicted in Figure 12a,b. The adherence and proliferation of the fibroblast cells on the surface of the MgHApCh composite thin films irradiated with a dose of 3 Gy of gamma radiation are depicted in the 2D AFM topography and its 3D representation from Figure 12c,d, and the 2D topography and corresponding 3D representation of the fibroblast

cells adhered to the surface of MgHApCh composite thin films irradiated with a dose of 3 Gy of gamma radiation are presented in Figure 12e,f.

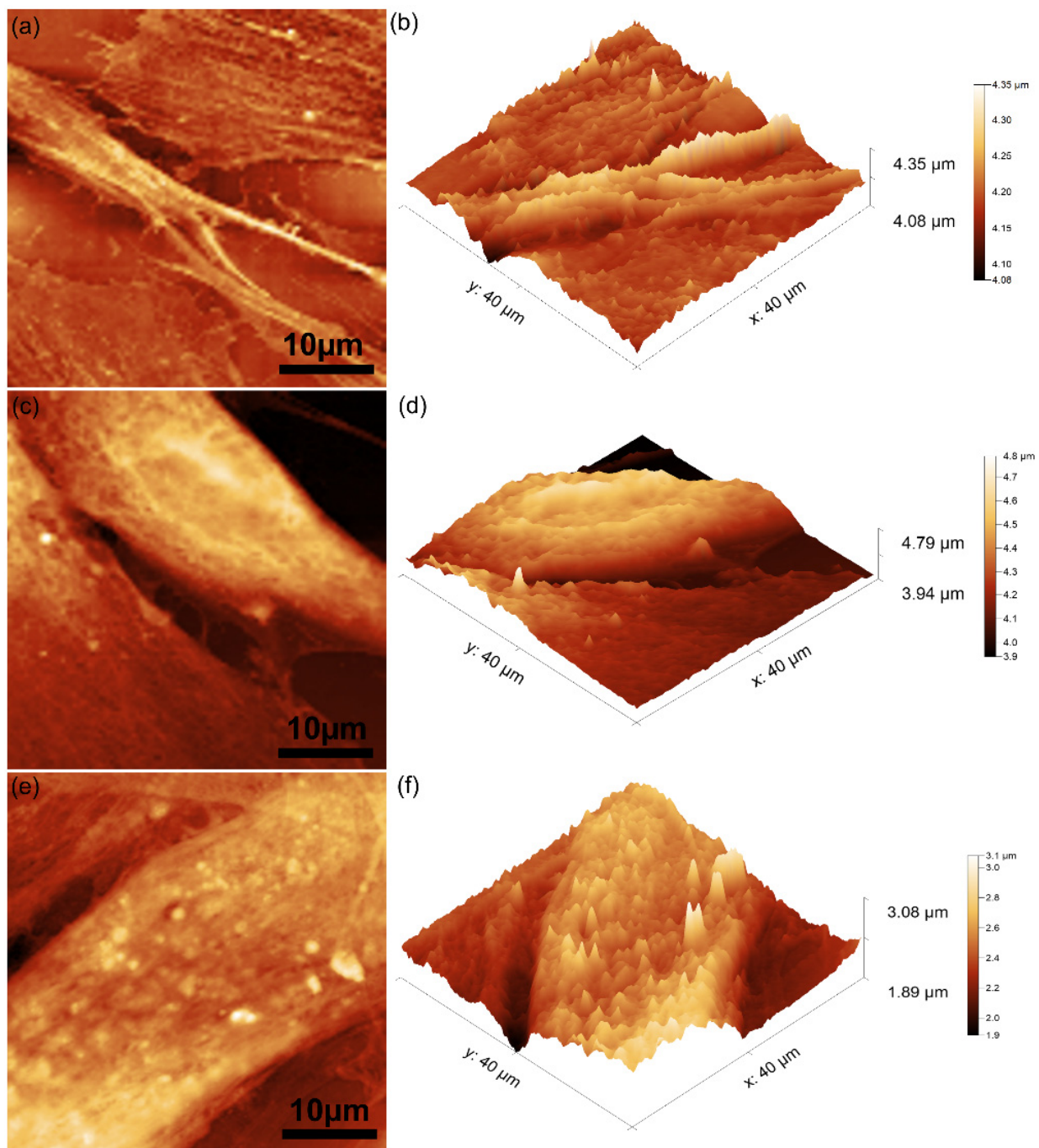


**Figure 12.** Two-dimensional AFM topography of fibroblast cells after 24 h of incubation with MgHApCh-0 (a), MgHApCh-3 composite thin film (c), and MgHApCh-6 composite thin film (e) and their 3D representation (b,d,f).

The AFM 2D topographies suggested that on the surface of the MgHApCh composite thin films could be found the typical patterns of the cellular morphology of fibroblast cells presenting morphologies of flattened cells varying from spindle-like to tile-like [62–67]. In addition, both the 2D AFM topographies and their 3D representations highlighted that after an incubation period of 24 h, the fibroblast cells had a very good adherence to the studied MgHApCh composite thin film surfaces. Moreover, the 2D AFM topographies

emphasized that the cells adhered and spread on the surface of the investigated MgHApCh composite thin films. The fibroblast cells measure several hundreds of micrometers, which exceed the normal range of an AFM scan. For this reason, the topographies presented in Figure 12a–f only depict parts of the cells that are attached to the surface of the MgHApCh composite thin films. Nonetheless, the AFM images demonstrated that the fibroblast cells adhered to the surface of the thin films. Moreover, the AFM 2D topographies suggested that the fibroblast cell adhesion and proliferation onto the MgHApCh composite thin films was influenced by the dose of gamma irradiation applied to the thin film. The AFM results highlighted that in the case of MgHApCh composite thin films irradiated with a dose of 6 Gy gamma radiation, the fibroblast cells spread on the surface and formed a monolayer of cells having the typical characteristic of an elongated fibroblastic morphology [68–79]. The results obtained by AFM investigation are in good agreement with the MTT cell viability assays and suggest that MgHApCh composite thin films do not have any cytotoxic effect against fibroblast cells after a period of incubation of 24 h, rendering them suitable for being employed in the development of biomedical devices.

Hydroxyapatite (HAp) is recognized as one of the best candidates that can be used to cover biomedical metal implants in order to improve the interaction between the implant and the host tissue. Because pure HAp coatings have relatively high in vivo solubility, attempts have been made to replace calcium in the crystal lattice of HAp with different ions to reduce long-term stability problems [80,81]. In this study, calcium ions in the crystal lattice were replaced with magnesium ions. Through this study, we tried to provide as much information as possible regarding the effect of irradiation on the surface of the MgHApCh thin layers obtained by vacuum deposition. Previous studies [82,83] have shown that techniques such as FTIR and XRD cannot provide the information needed to see the difference between the composition of the outer layer and the bulk. On the other hand, this study provides information on the influence of gamma irradiation on the biological properties of MgHApCh thin layers. The synthesis process for obtaining the necessary powders for the preparation of thin layers plays an important role [84]. Since the influence of surface impurities on the bioceramic plays an important role in biomedical implants, the surface composition of MgHApCh thin layers at the nanoscale was evaluated using XPS analysis. The peak of Ca 2p (for MgHApCh-6 composite thin films) at a BE of 347.50–347.80 eV associated for Ca–O was in good accordance with anterior studies [58–60]. A P 2p BE of 133.64 eV (for MgHApCh-6 composite thin films) corresponds to (–P=O) in  $\text{PO}_4^{3-}$  in agreement with previous results reported in the literature [60]. These results show that the substitution of calcium with magnesium atoms influences the Ca–O bond lengths and P–O bond lengths. An XPS study for the Mg 1s region showed a single peak at a position of 1304 eV, which fits well with the MgO structure [85]. The position of Mg 1s peak centered at a BE of 1302–1304 eV indicates the presence of MgO. In addition, we evaluated the chemical nature of Mg through the analysis of the principal Mg KLL Auger peak, which has a large chemical shift and is useful for chemical state analysis. Thus, Figure 9 shows the spectra of the Mg KLL Auger peak in the first 20 levels (up to 200 s of etching). We observed the peak centered at ~304–306 eV, corresponding to MgO. Moreover, in the peak centered at a BE of ~301 eV corresponding to the elementary Mg, no statistically significant signal was detected [86]. The presence of TCP was observed in gamma-irradiated samples. The amount of TCP was higher in the case of the MgHApCh-6 sample. The results obtained from the XPS analysis were in good agreement with those obtained from the EDS studies. SEM and AFM studies have also shown that porosity increases with increasing gamma radiation dose from 3 at 6 Gy.

The in vitro cell viability evaluation results showed that thin films composed of non-irradiated and irradiated MgHApCh (MgHApCh-3 and MgHApCh-6) have a very good viability in the presence of human fibroblast cells after a 24 h incubation period. This behavior was also demonstrated by the 2D AFM topographies, as well as their 3D representations. AFM studies have shown that human fibroblast cells have a very good adhesion to the surface of all samples studied. Both studies showed that the radiation dose previously

applied to thin composite films had a positive influence on the viability of fibroblast cells. If in the case of the MgHApCh-0 sample the fibroblast cells show flattened cell morphologies ranging from spindle-like to tile-like in the case of thin layers previously irradiated with a dose of gamma radiation of 6 Gy (MgHApCh-6), the fibroblast cells have an elongated morphology. Moreover, in the case of the MgHApCh-6 sample, the fibroblast cells spread on the surface, forming a monolayer of cells. This behavior is due to the presence of TCP in the top layer of the irradiated samples. As previously observed [26,54], the hydroxyapatite doped with different ions remained nontoxic even after the addition of these ions (Ag, Zn, Mg, Sm, etc.). In the case of MgHApCh thin films, the biocompatibility of chitosan-coated magnesium-doped hydroxyapatite is improved after irradiation due to the presence of TCP.

The development of chitosan-coated magnesium-doped hydroxyapatite thin films (MgHApCh) by the vacuum deposition method allowed us to study their surface before and after  $\gamma$ -irradiation. The incorporation of MgHAp in chitosan has led to changes in the surface of obtained thin films after irradiation as a result of chitosan-induced interactions upon irradiation. In agreement with the previous studies [87], the surface structure of the thin films plays a significant role in increasing the biocompatibility and the corrosion resistance of the implants. Moreover, the coating technique plays a very important role in terms of surface properties. In our previous studies [30], the MgHApCh layers obtained using magnetron sputtering technique showed a different behavior after irradiation. After irradiation with electron beams, the surface of layers became nanosized structured, and the peak broadening of the MgHApCh layers decreased with the increase in irradiation dose [30]. The irradiation of MgHApCh layers may improve the biological properties, and presence of Mg also provides considerable reinforcement to HAp. Studies conducted by Elayaraja et al. [88] on the enhancement of wettability and antibiotic loading/release of hydroxyapatite thin film modified by 100 MeV  $\text{Ag}^{7+}$  ion irradiation showed that the irradiation of  $\text{Ag}^{7+}$  ion on HAp thin film increased the biological performance. The chitosan-coated magnesium-doped hydroxyapatite thin films (MgHApCh) obtained by vacuum deposition method highlighted the presence of TCP in gamma-irradiated samples. The XPS and EDS studies showed that the presence of TCP was higher in the case of the MgHApCh-6 sample. On the other hand, an increase in porosity was observed when the samples were irradiated. Even if a significant variation of the Ca/P ratio was not observed after irradiation, a slight displacement of the peaks in the FTIR and XPS spectra and a peak broadening of the XRD were highlighted, which shows that after irradiation, the HAp unit cell was affected. Thus, MgHApCh thin films became amorphous after irradiation in agreement with previous research [88]. Due to the decreased crystallinity of the MgHApCh film after irradiation, it was observed that the adhesion of fibroblast cells increased. In the presence of irradiated MgHApCh thin films with a dose of gamma radiation of 6 Gy, the fibroblast cells formed a monolayer with a characteristic elongated shape.

The presence of TCP on the top layer of the irradiated samples favored the attachment of fibroblast cells to the surface of MgHApCh thin films, which offers the possibility of developing new generations of implantable materials with improved biological properties. Compared with previous research, this study approached a new method for obtaining biocompatible coatings based on magnesium-doped hydroxyapatite coated with chitosan. As a conclusion of the results obtained, the materials analyzed in this study could be implanted for bone repair.

#### 4. Conclusions

In the present study, for the first time, the effectiveness of vacuum deposition method for the preparation of chitosan-coated magnesium-doped hydroxyapatite  $\text{Ca}_{10-x}\text{Mg}_x(\text{PO}_4)_6(\text{OH})_2$  with  $x_{\text{Mg}} = 0.025$  (MgHApCh) composite thin films was demonstrated. The obtained samples were exposed to three irradiation doses (0, 3, and 6 Gy) of gamma irradiation. The MgHApCh composite thin films nonirradiated and irradiated were evaluated by X-ray diffraction (XRD), Fourier-transform infrared spectroscopy (FTIR), scanning electron microscopy (SEM), atomic force microscopy (AFM), and X-ray photoelectron spectroscopy

(XPS) in studies. Furthermore, the biological evaluations of these samples were conducted. The results of this study indicated that the vacuum deposition method allowed for obtaining uniform and homogeneous layers. The MgHApCh composite thin films with doses of 3 Gy of gamma irradiation remain uniform and homogeneous. Fine cracks appear on the MgHApCh composite thin films with doses of 6 Gy of gamma irradiation. A cellular viability similar to that of the control was observed for MgHApCh composite thin films with doses of 0 and 3 Gy of gamma irradiation. Moreover, the samples with doses of 6 Gy of gamma irradiation did not cause significantly higher cell death than the control ( $p > 0.05$ ). The homogeneous distribution of the pores that appeared on the surface of the thin film with doses of 6 Gy of gamma irradiation did not prevent the adhesion of the fibroblast cells and their spread on the coating. Our results suggest that by vacuum deposition method could be obtained thin films that may be suitable for use in bone implant and other orthopedic surgery interventions. Future studies will focus on obtaining biocompatible composite coatings with superior properties (such as surface with no defects after exposure to gamma irradiation) in order to increase their range of applicability.

**Author Contributions:** Conceptualization, D.P., C.S.C., S.L.I., S.R. and K.R.; methodology, D.P., C.S.C., S.L.I., S.R., M.L.B. and K.R.; software, D.P., S.L.I. and K.R.; validation, D.P., C.S.C., S.L.I., S.R., M.L.B. and K.R.; formal analysis, D.P., C.S.C., S.L.I., S.R., M.L.B. and K.R.; investigation, D.P., C.S.C., S.L.I., S.R., M.L.B. and K.R.; resources, D.P.; data curation, D.P., C.S.C., S.L.I., S.R., M.L.B. and K.R.; writing—original draft preparation, D.P., C.S.C., S.L.I. and K.R.; writing—review and editing, D.P., C.S.C., S.L.I., S.R. and K.R.; visualization, D.P., C.S.C., S.L.I., S.R., M.L.B. and K.R.; supervision, D.P., S.R. and K.R.; project administration, D.P. and K.R.; funding acquisition, D.P. and K.R. All authors have read and agreed to the published version of the manuscript.

**Funding:** This work was supported by the Romanian Ministry of Research and Innovation through the project PN-III-P2-2.1-PED-2019-0868, contract number 467PED2020.

**Institutional Review Board Statement:** Not applicable.

**Informed Consent Statement:** Not applicable.

**Data Availability Statement:** Not applicable.

**Acknowledgments:** We would like to thank Rodica V. Ghita for her help with the irradiation.

**Conflicts of Interest:** The authors declare no conflict of interest. The funders had no role in the design of the study; in the collection, analyses, or interpretation of data; in the writing of the manuscript; or in the decision to publish the results.

## References

1. Mousavi, S.M.; Esmaeili, H.; Arjmand, O.; Karimi, S.; Hashemi, S.A. Biodegradation Study of Nanocomposites of Phenol Novolac Epoxy/Unsaturated Polyester Resin/Egg Shell Nanoparticles Using Natural Polymers. *J. Mater.* **2015**, *2015*, 131957. [[CrossRef](#)]
2. Seyed, M.M. Unsaturated polyester resins modified with cresol novolac epoxy and silica nanoparticles: Processing and mechanical properties. *J. Chem. Pet. Eng.* **2016**, *5*, 13–26.
3. Mousavi, S.M.; Arjmand, O.; Hashemi, S.A.; Banaei, N. Modification of the Epoxy Resin Mechanical and Thermal Properties with Silicon Acrylate and Montmorillonite Nanoparticles. *Polym. Renew. Resour.* **2016**, *7*, 101–113. [[CrossRef](#)]
4. Mousavi, S.M.; Hashemi, S.A.; Jahandideh, S.; Baseri, S.; Zarei, M.; Azadi, S. Modification of Phenol Novolac Epoxy Resin and Unsaturated Polyester Using Sasobit and Silica Nanoparticles. *Polym. Renew. Resour.* **2017**, *8*, 117–132. [[CrossRef](#)]
5. Mousavi, S.M.; Hashemi, S.A.; Ramakrishna, S.; Esmaeili, H.; Bahrani, S.; Koosha, M.; Babapoor, A. Green synthesis of supermagnetic Fe<sub>3</sub>O<sub>4</sub>–MgO nanoparticles via Nutmeg essential oil toward superior anti-bacterial and anti-fungal performance. *J. Drug Deliv. Sci. Technol.* **2019**, *54*, 101352. [[CrossRef](#)]
6. Ahmadi, S.; Fazilati, M.; Mousavi, S.M.; Nazem, H. Anti-bacterial/fungal and anti-cancer performance of green synthesized Ag nanoparticles using summer savory extract. *J. Exp. Nanosci.* **2020**, *15*, 363–380. [[CrossRef](#)]
7. Mousavi, S.M.; Hashemi, S.A.; Zarei, M.; Gholami, A.; Lai, C.W.; Chiang, W.H.; Omidifar, N.; Bahrani, S.; Mazraedoost, S. Recent Progress in Chemical Composition, Production, and Pharmaceutical Effects of Kombucha Beverage: A Complementary and Alternative Medicine. *Evid. Based Complement. Altern. Med.* **2020**, *2020*, 4397543. [[CrossRef](#)]
8. Ahmadi, S.; Fazilati, M.; Nazem, H.; Mousavi, S.M. Green Synthesis of Magnetic Nanoparticles Using Satureja hortensis Essential Oil toward Superior Antibacterial/Fungal and Anticancer Performance. *BioMed Res. Int.* **2021**, *2021*, 8822645. [[CrossRef](#)]



9. Abootalebi, S.N.; Mousavi, S.M.; Hashemi, S.A.; Shorafa, E.; Omidifar, N.; Gholami, A. Antibacterial Effects of Green-Synthesized Silver Nanoparticles Using *Ferula asafoetida* against *Acinetobacter baumannii* Isolated from the Hospital Environment and Assessment of Their Cytotoxicity on the Human Cell Lines. *J. Nanomater.* **2021**, *2021*, 6676555. [[CrossRef](#)]
10. Gholami, A.; Mousavi, S.M.; Hashemi, S.A.; Ghasemi, Y.; Chiang, W.H.; Parvin, N. Current trends in chemical modifications of magnetic nanoparticles for targeted drug delivery in cancer chemotherapy. *Drug Metab. Rev.* **2020**, *52*, 205–224. [[CrossRef](#)]
11. Mousavi, S.M.; Zarei, M.; Hashemi, S.A.; Ramakrishna, S.; Chiang, W.H.; Lai, C.W.; Gholami, A. Gold nanostars-diagnosis, bioimaging and biomedical applications. *Drug Metab. Rev.* **2020**, *52*, 299–318. [[CrossRef](#)] [[PubMed](#)]
12. Mousavi, S.M.; Hashemi, S.A.; Zarei, M.; Bahrani, S.; Savardashtaki, A.; Esmaeili, H.; Lai, C.W.; Mazraedoost, S.; Abassi, M.; Ramavandi, B. Data on cytotoxic and antibacterial activity of synthesized Fe<sub>3</sub>O<sub>4</sub> nanoparticles using *Malva sylvestris*. *Data Brief* **2019**, *28*, 104929. [[CrossRef](#)] [[PubMed](#)]
13. Gholami, A.; Hashemi, S.A.; Yousefi, K.; Mousavi, S.M.; Chiang, W.H.; Ramakrishna, S.; Mazraedoost, S.; Alizadeh, A.; Omidifar, N.; Behbudi, G.; et al. 3D Nanostructures for Tissue Engineering, Cancer Therapy, and Gene Delivery. *J. Nanomater.* **2020**, *2020*, 1852946. [[CrossRef](#)]
14. Mousavi, S.M.; Zarei, M.; Hashemi, S.A.; Ramakrishna, S.; Chiang, W.-H.; Lai, C.W.; Gholami, A.; Omidifar, N.; Shokripour, M. Asymmetric Membranes: A Potential Scaffold for Wound Healing Applications. *Symmetry* **2020**, *12*, 1100. [[CrossRef](#)]
15. Mousavi, S.M.; Hashemi, S.A.; Gholami, A.; Omidifar, N.; Zarei, M.; Bahrani, S.; Yousefi, K.; Chiang, W.-H.; Babapoor, A. Bioinorganic synthesis of polyrhodanine stabilized Fe<sub>3</sub>O<sub>4</sub>/Graphene oxide in microbial supernatant media for anticancer and antibacterial applications. *Bioinorg. Chem. Appl.* **2021**, *2021*, 9972664. [[CrossRef](#)]
16. Vallet-Regi, M.; González-Calbet, J.M. Calcium phosphates as substitution of bone tissues. *Prog. Solid State Chem.* **2004**, *32*, 1–31. [[CrossRef](#)]
17. Joshy, M.A.; Kolanthai, E.; Kumar, V.S.; Sindu, P.A.; Asokan, K.; Kalkura, S.N. Investigations on the effect of swift heavy silicon ion irradiation on hydroxyapatite. *Mater. Today Proc.* **2021**, *28*, 802–811. [[CrossRef](#)]
18. Abutalib, M.M.; Yahia, I.S. Novel and facile microwave-assisted synthesis of Mo-doped hydroxyapatite nanorods: Characterization, gamma absorption coefficient, and bioactivity. *Mater. Sci. Eng. C* **2017**, *78*, 1093–1100. [[CrossRef](#)]
19. Saravanan, S.; Leena, R.; Selvamurugan, N. Chitosan based biocomposite scaffolds for bone tissue engineering. *Int. J. Biol. Macromol.* **2016**, *93*, 1354–1365. [[CrossRef](#)]
20. Sedghi, R.; Shaabani, A.; Mohammadi, Z.; Samadi, F.Y.; Isaei, E. Biocompatible electrospinning chitosan nanofibers: A novel delivery system with superior local cancer therapy. *Carbohydr. Polym.* **2017**, *159*, 1–10. [[CrossRef](#)]
21. Rezaei, F.S.; Sharifianjazi, F.; Esmaeilkhani, A.; Salehi, E. Chitosan films and scaffolds for regenerative medicine applications: A review. *Carbohydr. Polym.* **2021**, *273*, 118631. [[CrossRef](#)] [[PubMed](#)]
22. Ran, J.; Jiang, P.; Sun, G.; Ma, Z.; Hu, J.; Shen, X.; Tong, H. Comparisons among Mg, Zn, Sr, and Si doped nano-hydroxyapatite/chitosan composites for load-bearing bone tissue engineering applications. *Mater. Chem. Front.* **2017**, *1*, 900–910. [[CrossRef](#)]
23. Huang, J.; Best, S.; Brooks, R.; Rushton, N.; Bonfield, W. In vitro evaluation of nanosized carbonate-substituted hydroxyapatite and its polyhydroxyethylmethacrylate nanocomposite. *J. Biomed. Mater. Res. Part A* **2008**, *87*, 598–607. [[CrossRef](#)] [[PubMed](#)]
24. Wu, S.; Liu, X.; Yeung, K.W.K.; Liu, C.; Yang, X. Biomimetic porous scaffolds for bone tissue engineering. *Mater. Sci. Eng. R Rep.* **2014**, *80*, 1–36. [[CrossRef](#)]
25. Mansour, S.F.; El-Dek, S.I.; Dorozhkin, S.V.; Ahmed, M.K. Physico-mechanical properties of Mg and Ag doped hydroxyapatite/chitosan biocomposites. *N. J. Chem.* **2017**, *41*, 13773–13783. [[CrossRef](#)]
26. Predoi, D.; Iconaru, S.L.; Predoi, M.V. Fabrication of Silver- and Zinc-Doped Hydroxyapatite Coatings for Enhancing Antimicrobial Effect. *Coatings* **2020**, *10*, 905. [[CrossRef](#)]
27. Vladescu, A.; Cotrut, C.M.; Azem, F.A.; Bramowicz, M.; Pana, I.; Braic, V.; Birlik, I.; Kiss, A.; Braic, M.; Abdulgader, R.; et al. Sputtered Si and Mg doped hydroxyapatite for biomedical applications. *Biomed. Mater.* **2018**, *13*, 025011. [[CrossRef](#)]
28. Becker, A.; Ziegler, A.; Epple, M. The mineral phase in the cuticles of two species of Crustacea consists of magnesium calcite, amorphous calcium carbonate, and amorphous calcium phosphate. *Dalton Trans.* **2005**, *10*, 1814–1820. [[CrossRef](#)]
29. Jenifer, A.; Senthilarasan, K.; Arumugam, S.; Sivaprakash, P.; Sagadevan, S.; Sakthivel, P. Investigation on antibacterial and hemolytic properties of magnesium-doped hydroxyapatite nanocomposite. *Chem. Phys. Lett.* **2021**, *771*, 138539. [[CrossRef](#)]
30. Bitu, B.; Stancu, E.; Stroe, D.; Dumitrache, M.; Ciobanu, S.C.; Iconaru, S.L.; Predoi, D.; Groza, A. The Effects of Electron Beam Irradiation on the Morphological and Physicochemical Properties of Magnesium-Doped Hydroxyapatite/Chitosan Composite Coatings. *Polymers* **2022**, *14*, 582. [[CrossRef](#)]
31. Abdullahi, I.; Zainol, I. Synthesis, Characterization and In vitro Bioactivity of Chitosan-Hydroxyapatite Composite Doped with Magnesium. *J. Chem. Soc. Nigeria* **2019**, *44*, 1268–1275. [[CrossRef](#)]
32. Predoi, D.; Iconaru, S.L.; Predoi, M.V.; Buton, N.; Motelica-Heino, M. Zinc Doped Hydroxyapatite Thin Films Prepared by Sol-Gel Spin Coating Procedure. *Coatings* **2019**, *9*, 156. [[CrossRef](#)]
33. Sutha, S.; Dhineshababu, N.R.; Prabhu, M.; Rajendran, V. Mg-Doped Hydroxyapatite/Chitosan Composite Coated 316L Stainless Steel Implants for Biomedical Applications. *J. Nanosci. Nanotechnol.* **2015**, *15*, 4178–4187. [[CrossRef](#)] [[PubMed](#)]
34. Negrila, C.C.; Predoi, D.; Ghita, R.V.; Iconaru, S.L.; Ciobanu, S.C.; Manea, M.; Badea, M.L.; Costescu, A.; Trusca, R.; Predoi, G.; et al. Multi-Level Evaluation of UV Action upon Vitamin D Enhanced, Silver Doped Hydroxyapatite Thin Films Deposited on Titanium Substrate. *Coatings* **2021**, *11*, 120. [[CrossRef](#)]

35. Mroz, W.; Jedynski, M.; Prokopiuk, A.; Slosarczyk, A.; Paszkiewicz, Z. Characterization of calcium phosphate coatings doped with Mg, deposited by pulsed laser deposition technique using ArF excimer laser. *Micron* **2009**, *40*, 140–142. [CrossRef]
36. Predoi, D.; Iconaru, S.L.; Predoi, M.V.; Groza, A.; Gaiaschi, S.; Rokosz, K.; Raaen, S.; Negrila, C.C.; Prodan, A.-M.; Costescu, A.; et al. Development of Cerium-Doped Hydroxyapatite Coatings with Antimicrobial Properties for Biomedical Applications. *Coatings* **2020**, *10*, 516. [CrossRef]
37. Predoi, D.; Ghita, R.V.; Ungureanu, F.; Negrila, C.C.; Vatasescu-Balcan, R.A.; Costache, M. Characteristics of hydroxyapatite thin films. *J. Optoelectron. Adv. Mater.* **2007**, *9*, 3827.
38. Teng, S.H.; Lee, E.J.; Wang, P.; Shin, D.S.; Kim, H.E. Three-layered membranes of collagen/hydroxyapatite and chitosan for guided bone regeneration. *J. Biomed. Mater. Res. B Appl. Biomater.* **2008**, *87*, 132–138. [CrossRef]
39. Pistone, A.; Iannazzo, D.; Celesti, C.; Piperopoulos, E.; Ashok, D.; Cembran, A.; Tricoli, A.; Nisbet, D. Engineering of Chitosan-Hydroxyapatite-Magnetite Hierarchical Scaffolds for Guided Bone Growth. *Materials* **2019**, *12*, 2321. [CrossRef]
40. Banerjee, S.; Bagchi, B.; Bhandary, S.; Kool, A.; Hoque, N.A.; Biswas, P.; Pal, K.; Thakur, P.; Das, K.; Karmakar, P.; et al. Antimicrobial and biocompatible fluorescent hydroxyapatite-chitosan nanocomposite films for biomedical applications. *Colloids Surf. B Biointerfaces* **2018**, *171*, 300–307. [CrossRef]
41. Dadbin, S.; Kheirkhah, Y. Gamma irradiation of melt processed biomedical PDLA/HAP nanocomposites. *Radiat. Phys. Chem.* **2014**, *97*, 270–274. [CrossRef]
42. Lu, K.; Li, C.; Wang, H.Z.; Li, Y.L.; Zhu, Y.; Ouyang, Y. Effect of gamma irradiation on carbon dot decorated polyethylene-gold@hydroxyapatite biocomposite on titanium implanted repair for shoulder joint arthroplasty. *J. Photochem. Photobiol. B Biol.* **2019**, *197*, 111504. [CrossRef]
43. Predoi, D.; Iconaru, S.L.; Predoi, M.V.; Motelica-Heino, M.; Guegan, R.; Buton, N. Evaluation of Antibacterial Activity of Zinc-Doped Hydroxyapatite Colloids and Dispersion Stability Using Ultrasounds. *Nanomaterials* **2019**, *9*, 515. [CrossRef] [PubMed]
44. Groza, A.; Iconaru, S.L.; Jiga, G.; Chapon, P.; Gaiaschi, S.; Verga, N.; Beuran, M.; Prodan, A.M.; Matei, M.; Marinescu, S.A.; et al. The Effect of the Ionizing Radiation on Hydroxyapatite-Polydimethylsiloxane Layers. *Polym. Eng. Sci.* **2019**, *59*, 2406–2412. [CrossRef]
45. Predoi, D.; Iconaru, S.L.; Predoi, M.V.; Stan, G.E.; Buton, N. Synthesis, Characterization, and Antimicrobial Activity of Magnesium-Doped Hydroxyapatite Suspensions. *Nanomaterials* **2019**, *9*, 1295. [CrossRef]
46. Ciobanu, C.S.; Iconaru, S.L.; Popa, C.L.; Motelica-Heino, M.; Predoi, D. Evaluation of samarium doped hydroxyapatite, ceramics for medical application: Antimicrobial activity. *J. Nanomater.* **2015**, *2015*, 849216. [CrossRef]
47. ImageJ Website. Available online: <http://imagej.nih.gov/ij> (accessed on 29 January 2022).
48. Gwyddion. Available online: <http://gwyddion.net/> (accessed on 30 January 2022).
49. Iconaru, S.L.; Predoi, M.V.; Chapon, P.; Gaiaschi, S.; Rokosz, K.; Raaen, S.; Motelica-Heino, M.; Predoi, D. Investigation of Spin Coating Cerium-Doped Hydroxyapatite Thin Films with Antifungal Properties. *Coatings* **2021**, *11*, 464. [CrossRef]
50. Iconaru, S.L.; Groza, A.; Gaiaschi, S.; Rokosz, K.; Raaen, S.; Ciobanu, S.C.; Chapon, P.; Predoi, D. Antimicrobial Properties of Samarium Doped Hydroxyapatite Suspensions and Coatings. *Coatings* **2020**, *10*, 1124. [CrossRef]
51. Casa Software Ltd. CasaXPS: Processing Software for XPS, AES, SIMS and More. 2009. Available online: [www.casaxps.com](http://www.casaxps.com) (accessed on 20 February 2022).
52. Biesinger, M.C.; Lau, L.W.M.; Gerson, A.R.; Smart, R.S.C. Resolving surface chemical states in XPS analysis of first row transition metals, oxides and hydroxides: Sc, Ti, V, Cu and Zn. *Appl. Surf. Sci.* **2010**, *257*, 887–898. [CrossRef]
53. Wagner, C.D.; Naumkin, A.V.; Kraut-Vass, A.; Allison, J.W.; Powell, C.J.; Rumble, J.R., Jr. NIST Standard Reference Database 20, Version 3.4. 2003. Available online: [srdata.nist.gov/xps](http://srdata.nist.gov/xps) (accessed on 20 February 2022).
54. Nica, I.C.; Popa, M.; Marutescu, L.; Dinischiotu, A.; Iconaru, S.L.; Ciobanu, S.C.; Predoi, D. Biocompatibility and Antibiofilm Properties of Samarium Doped Hydroxyapatite Coatings: An In Vitro Study. *Coatings* **2021**, *11*, 1185. [CrossRef]
55. Casaletto, M.P.; Kaciulis, S.; Mattogno, G.; Mezzi, A.; Ambrosio, L.; Branda, F. XPS characterization of biocompatible hydroxyapatite-polymer coatings. *Surf. Interface Anal.* **2013**, *34*, 45–49. [CrossRef]
56. Lebugle, A.; Rovira, A.; Rabaud, M.; Rey, C. XPS study of elastin-solubilized peptides binding onto apatite in orthopaedic biomaterials. *J. Mat. Sci. Mat. Med.* **1996**, *7*, 223–226. [CrossRef]
57. Maachou, H.; Genet, M.J.; Aliouche, D.; Dupont-Gillain, C.C.; Rouxhet, P.G. XPS analysis of chitosan-hydroxyapatite biomaterials: From elements to compounds. *Surf. Interface Anal.* **2013**, *45*, 1088–1095. [CrossRef]
58. Stipp, S.L.; Hochella, M.F. Structure and bonding environments at the calcite surface as observed with X-ray photoelectron spectroscopy (XPS) and low energy electron diffraction (LEED). *Geochim. Cosmochim. Acta* **1991**, *55*, 1723–1736. [CrossRef]
59. Ni, M.; Ratner, B.D. Differentiating calcium carbonate polymorphs by surface analysis techniques—an XPS and TOF-SIMS study. *Surf. Interface Anal.* **2008**, *40*, 1356–1361. [CrossRef]
60. Kaciulis, S.; Mattogno, G.; Pandolfi, L.; Cavalli, M.; Gnappi, G.; Montenero, A. XPS study of apatite-based coatings prepared by sol-gel technique. *Appl. Surf. Sci.* **1999**, *151*, 1–5. [CrossRef]
61. Boanini, E.; Gazzano, M.; Nervi, C.; Chierotti, M.R.; Rubini, K.; Gobetto, R.; Bigi, A. Strontium and Zinc Substitution in  $\beta$ -Tricalcium Phosphate: An X-ray Diffraction, Solid State NMR and ATR-FTIR Study. *J. Funct. Biomater.* **2019**, *10*, 20. [CrossRef]

62. Braet, F.; de Zanger, R.; Seynaeve, C.; Baekeland, M.; Wisse, E. A comparative atomic force microscopy study on living skin fibroblasts and liver endothelial cells. *Microscopy* **2001**, *50*, 283–290. [[CrossRef](#)]
63. Bushell, G.R.; Cahill, C.; Clarke, F.M.; Gibson, C.T.; Myhra, S.; Watson, G.S. Imaging and force-distance analysis of human fibroblasts in vitro by atomic force microscopy. *Cytom. J. Int. Soc. Anal. Cytol.* **1999**, *36*, 254–264. [[CrossRef](#)]
64. Silva, W.D.M.; Ribeiro, C.A.; Marques, C.S.; Tabata, A.S.; Saeki, M.J.; Medeiros, L.I.; Oliveira, D.E.D. Fibroblast and pre-osteoblast cell adhesive behavior on titanium alloy coated with diamond film. *Mater. Res.* **2017**, *20*, 284–290. [[CrossRef](#)]
65. Akhatova, F.; Ishmukhametov, I.; Fakhruullina, G.; Fakhruullin, R. Nanomechanical Atomic Force Microscopy to Probe Cellular Microplastics Uptake and Distribution. *Int. J. Mol. Sci.* **2022**, *23*, 806. [[CrossRef](#)] [[PubMed](#)]
66. Lee, G.J.; Uhm, Y.K.; Eo, Y.H.; Park, J.H.; Lim, J.E.; Jo, T.H.; Kim, B.S.; Choi, S.K.; Oh, B.S.; Lee, M.H.; et al. Optimization of wet fixation methods for AFM imaging of human fibroblast cells. *Exp. Neurobiol.* **2008**, *17*, 17–24. [[CrossRef](#)]
67. Binnig, G.; Quate, C.F.; Gerber, C.H. Atomic force microscope. *Phys. Rev. Lett.* **1986**, *56*, 930–933. [[CrossRef](#)]
68. Ramya, J.R.; Arul, K.T.; Sathiamurthi, P.; Nivethaa, E.A.K.; Baskar, S.; Amudha, S.; Mohana, B.; Elayaraja, K.; Veerla, S.C.; Asokan, K.; et al. Gamma irradiated poly (methyl methacrylate)-reduced graphene oxide composite thin films for multifunctional applications. *Compos. Part B Eng.* **2019**, *163*, 752–760. [[CrossRef](#)]
69. Ramya, J.R.; Arul, K.T.; Sathiamurthi, P.; Asokan, K.; Singh, N.R.; Kalkura, S.N. Enhanced magnetic behaviour and cell proliferation of gamma irradiated dual metal ions co-doped hydroxyapatite-poly(methyl methacrylate) composite films. *React. Funct. Polym.* **2018**, *123*, 34–43. [[CrossRef](#)]
70. Latifi, N.; Asgari, M.; Vali, H.; Mongeau, L. A tissue-mimetic nano-fibrillar hybrid injectable hydrogel for potential soft tissue engineering applications. *Sci. Rep.* **2018**, *8*, 1047. [[CrossRef](#)]
71. Karthika, A.; Kavitha, L.; Surendiran, M.; Kannanc, S.; Gopi, D. Fabrication of divalent ion substituted hydroxyapatite/gelatin nanocomposite coating on electron beam treated titanium: Mechanical, anticorrosive, antibacterial and bioactive evaluations. *RSC Adv.* **2015**, *5*, 47341–47352. [[CrossRef](#)]
72. Ghobashy, M.M.; El-Sawy, N.M.; Kodous, A.S. Nanocomposite of cosubstituted carbonated hydroxyapatite fabricated inside Poly(sodium hyaluronate-acrylamide) hydrogel template prepared by gamma radiation for osteoblast cell regeneration. *Radiat. Phys. Chem.* **2021**, *183*, 109408. [[CrossRef](#)]
73. Donaubaue, A.-J.; Deloch, L.; Becker, I.; Fietkau, R.; Frey, B.; Gaip, U.S. The Influence of Radiation on Bone and Bone Cells—Differential Effects on Osteoclasts and Osteoblasts. *Int. J. Mol. Sci.* **2020**, *21*, 6377. [[CrossRef](#)]
74. Ramya, J.R.; Arul, K.T.; Sathiamurthi, P.; Asokan, K.; Kalkura, S.N. Novel gamma irradiated agarose-gelatin-hydroxyapatite nanocomposite scaffolds for skin tissue regeneration. *Ceram. Int.* **2016**, *42*, 11045–11054. [[CrossRef](#)]
75. Chung, R.J.; Hsieh, M.F.; Huang, C.W.; Perng, L.H.; Wen, H.W.; Chin, T.S. Antimicrobial effects and human gingival biocompatibility of hydroxyapatite sol-gel coatings. *J. Biomed. Mater. Res.* **2006**, *76*, 169–178. [[CrossRef](#)]
76. Murphy, M.F.; Lalor, M.J.; Manning, F.C.; Lilley, F.; Crosby, S.R.; Randall, C.; Burton, D.R. Comparative study of the conditions required to image live human epithelial and fibroblast cells using atomic force microscopy. *Microsc. Res. Tech.* **2006**, *69*, 757–765. [[CrossRef](#)]
77. Rotsch, C.; Radmacher, M. Drug-induced changes of cytoskeletal structure and mechanics in fibroblasts: An atomic force microscopy study. *Biophys. J.* **2000**, *78*, 520–535. [[CrossRef](#)]
78. Deligianni, D.D.; Katsala, N.D.; Koutsoukos, P.G.; Missirlis, Y.F. Effect of surface roughness of hydroxyapatite on human bone marrow cell adhesion, proliferation, differentiation and detachment strength. *Biomaterials* **2001**, *22*, 87–96. [[CrossRef](#)]
79. Kim, M.H.; Kim, B.S.; Lee, J.; Cho, D.; Kwon, O.H.; Park, W.H. Silk fibroin/hydroxyapatite composite hydrogel induced by gamma-ray irradiation for bone tissue engineering. *Biomater. Res.* **2017**, *21*, 12. [[CrossRef](#)]
80. Gineste, L.; Gineste, M.; Ranz, X.; Ellefterion, A.; Guilhem, A.; Rouquet, N.; Frayssinet, P. Degradation of hydroxyapatite, fluorapatite, and fluorhydroxyapatite coatings of dental implants in dogs. *J. Biomed. Mater. Res.* **1999**, *48*, 224–234. [[CrossRef](#)]
81. Overgaard, S.; Lind, M.; Josephsen, K.; Maunsbach, A.B.; Bünger, C.; Søballe, K. Resorption of hydroxyapatite and fluorapatite ceramic coatings on weight-bearing implants: A quantitative and morphological study in dogs. *J. Biomed. Mater. Res.* **1998**, *39*, 141–152. [[CrossRef](#)]
82. França, R.; Mbeh, D.A.; Samani, T.D.; Le Tien, C.; Mateescu, M.A.; Yahia, L.; Sacher, E. The effect of ethylene oxide sterilization on the surface chemistry and in vitro cytotoxicity of several kinds of chitosan. *J. Biomed. Mater. Res. B Appl. Biomater.* **2013**, *101*, 1444–1455. [[CrossRef](#)]
83. Mbeh, D.A.; França, R.; Merhi, Y.; Zhang, X.F.; Veres, T.; Sacher, E.; Yahia, L. In vitro biocompatibility assessment of functionalized magnetite nanoparticles: Biological and cytotoxicological effects. *J. Biomed. Mater. Res. Part A* **2012**, *100*, 1637–1646. [[CrossRef](#)]
84. Cuneyt Tas, A.; Korkusuz, F.; Timucin, M.; Akkas, N. An investigation of the chemical synthesis and high-temperature sintering behaviour of calcium hydroxyapatite (HA) and tricalcium phosphate (TCP) bioceramics. *J. Mater. Sci. Mater. Med.* **1997**, *8*, 91–96. [[CrossRef](#)]
85. Gholinejad, M.; Bahrami, M.; Nájera, C. A fluorescence active catalyst support comprising carbon quantum dots and magnesium oxide doping for stabilization of palladium nanoparticles: Application as a recoverable catalyst for Suzuki reaction in water. *Mol. Catal.* **2017**, *433*, 12–19. [[CrossRef](#)]

86. Dubecký, F.; Kindl, D.; Hubík, P.; Mičušík, M.; Dubecký, M.; Boháček, P.; Vanko, G.; Gombia, E.; Nečas, V.; Mudroň, J. A comparative study of Mg and Pt contacts on semi-insulating GaAs: Electrical and XPS characterization. *Appl. Surf. Sci.* **2017**, *395*, 131–135. [[CrossRef](#)]
87. Capello, W.N.; D'Antonio, J.A.; Geesink, R.G.; Feinberg, J.R.; Naughton, M. Late Remodeling Around a Proximally HA-coated Tapered Titanium Femoral Component. *Clin. Orthop. Relat. Res.* **2009**, *467*, 155. [[CrossRef](#)]
88. Elayaraja, K.; Rajesh, P.; Ahymah Joshy, M.I.; Sarath Chandra, V.; Suganthi, R.V.; Kennedy, J.; Kulriya, P.K.; Sulania, I.; Asokan, K.; Kanjilal, D.; et al. Enhancement of wettability and antibiotic loading/release of hydroxyapatite thin film modified by 100 MeV  $\text{Ag}^{7+}$  ion irradiation. *Mater. Chem. Phys.* **2012**, *134*, 464–477. [[CrossRef](#)]